

# Two-component nanopillar arrays grown by Glancing Angle Deposition

S.V. Kesapragada, D. Gall\*

*Department of Materials Science and Engineering, Rensselaer Polytechnic Institute, Troy, NY 12180, United States*

Available online 13 September 2005

## Abstract

Periodic arrays of 160- to 500-nm-wide Si and Cr nanostructures were grown on patterned Si(001) substrates by Glancing Angle Deposition (GLAD). Initial patterning was achieved by colloidal self-assembly of 500-nm-diameter polystyrene and 160-nm-diameter silica microspheres which form, during drying from suspension, close-packed hexagonal arrays. Si deposition onto a monolayer of 500-nm-diameter spheres from an angle  $\alpha$ , with respect to the surface normal, of  $72^\circ$ , yields a regular array of 2- $\mu\text{m}$ -tall and 450-nm-wide nanopillars. Regular arrays of 300-nm-wide Cr nano-half-moon structures are obtained with  $\alpha = 86^\circ$ . Cr–Si two-component multi-stack nanopillars were grown on 160-nm-diameter nanospheres by successive Cr and Si deposition sequences with continuous rotation of the substrate about the polar axis. The resulting 300-nm-tall pillars have a large distribution in width, ranging from 120 to 170 nm, show height variations, and some randomness in arrangement. This is in strong contrast to nanostructures on 500-nm spheres which perfectly replicate the underlying microsphere array. The transition to a less ordered morphology is attributed to a competitive growth mode which becomes dominant when the pattern period is smaller than the length scales of surface diffusion and column self-shadowing. That is, in the case of 160-nm patterns, competition between neighboring columns causes exacerbated growth of some columns at the cost of others which die out. This competition is delayed for growth on 500-nm-diameter spheres, yielding regular nanostructure arrays.

© 2005 Elsevier B.V. All rights reserved.

*Keywords:* Surface patterning; Glancing Angle Deposition (GLAD); Column competition; Atomic shadowing

## 1. Introduction

Glancing Angle Deposition (GLAD) is a thin-film deposition technique where the deposition flux, consisting of atoms and molecules from gas phase, impinges on the substrate from oblique angles ( $\alpha$ ), resulting in highly underdense, columnar microstructures which are purposely engineered to achieve novel desired properties. GLAD has been known for several decades [1] but has recently drawn considerable attention due to the wide range of achievable nanostructures [2–26] with potential applications in optically active coatings [7], including polarizers [8], high birefringence biaxial films [9], thin film wave plates [10], helicoidal bianisotropic media [11,12], spectral hole filters [13,14], photonic crystals [15–17], magnetic storage media [18–21], and nanoemitters [26]. Sculptured thin films (STF)

containing engineered complex structures such as nanospirals [24] and zigzag columns [4] can be achieved by rotating the substrate about the polar axis in predefined cycles [4]. The polar angle ( $\phi$ ) determines the column growth direction while the azimuthal angle ( $\alpha$ ) controls the column tilt angle and affects the degree of shadowing and thus the porosity of the layer. GLAD on flat substrates involves a stochastic nucleation process yielding layers consisting of randomly distributed columns [27]. In contrast, periodic arrays are achieved by substrate patterning prior to deposition [27]. In this case, the patterned surface mounds are the nucleation sites for the GLAD columns, since atomic shadowing of the deposition flux suppresses growth on the surrounding substrate.

Most reported investigations on GLAD layers have been on sculptured columns consisting of only one particular material like Si [24], Co [24,28], W [24], Ta [19], and Cr [29]. In contrast, the use of multiple diverse materials within a single GLAD layer is almost completely unexplored. Such layers consisting of multi-component nano-

\* Corresponding author.

*E-mail address:* [galld@rpi.edu](mailto:galld@rpi.edu) (D. Gall).

columns that are shaped by the GLAD process are expected to enhance the complex functionality achieved by conventional single-component layers and may find applications as smart coatings, wear resistant hard coatings, and sensitive pressure sensor arrays.

This paper describes the growth and characterization of single-component Cr, Si and multi-component Cr–Si nanopillars. All the nanopillars were grown by ultra-high vacuum magnetron sputtering on Si (001) substrates patterned with 500 nm polystyrene (PS) and 160 nm silica microspheres. Two-micrometer-tall Si nanopillars and 300-nm-tall Cr nano-half-moon structures grown on 500 nm spheres exhibit regular close packed arrays. In contrast, Cr–Si multi-component nanopillars grown on 160-nm-diameter silica spheres have a large distribution in width, height, and interpillar spacing. We attribute the randomness of the pillar morphology on 160-nm patterns to a competitive growth mode caused by the smaller periodicity in comparison to the 500-nm-pattern. Scanning electron microscopy performed in secondary electron and back-scatter modes clearly shows the compositional contrast in the multi-component nanopillars.

## 2. Experimental procedure

Substrates were patterned using 160 to 500 nm diameter PS and SiO<sub>2</sub> spheres that self-assemble from colloidal suspensions according to the following procedure, adapted from Ref. [30]. Si (001) substrates were first cleaned by RCA cleaning [31] yielding OH<sup>−</sup> termination on the surface. A dispersion of PS microspheres (Alfa Aesar, 2.5 wt.%) was diluted in de-ionized water in a 1:10 ratio. A 5.6- $\mu$ l-drop of this colloidal suspension was then released on top of a 6.5-cm<sup>2</sup> substrate that was tilted at an angle of 10° with respect to the horizontal. The 10° inclination yields a flow gradient for the drying process that starts on the top of the substrate and continues to the bottom, resulting in a close-packed monolayer of nanospheres. Patterning with SiO<sub>2</sub> nanospheres was done with a similar procedure, as that described for PS, but instead of RCA cleaning, the Si wafers were cleaned in subsequent ultrasonic baths of isopropyl alcohol and acetone.

All films were grown in a load-locked ultrahigh vacuum (UHV) stainless steel dc magnetron sputter deposition system. The chamber has a base pressure of  $1.3 \times 10^{-7}$  Pa, maintained using a 520 l s<sup>−1</sup> turbo-molecular pump. The sample stage allows continuous polar rotation, external adjustment of azimuthal angle and heating up to 1200 °C. Water-cooled Si (99.999% pure) and Cr (99.95% pure) targets were mounted at an angle of 100° with respect to each other and with their surfaces being perpendicular to the substrate surface. This arrangement provides external control over the azimuthal deposition angle  $\alpha$ , from 60° to 90°, using a linear motion of the sample perpendicular to its surface. The Si substrates were attached to a molybdenum holder

using Pelco colloidal silver paste (Ted Pella, Inc.) and introduced into the chamber through the load lock. 99.99999% pure Ar was further purified using a Micro Torr purifier and introduced through metering valves to reach a constant pressure of 0.13 Pa (1.0 mTorr) in the chamber, which was measured using a capacitance manometer (Baratron) and held constant during all deposition steps. The targets were sputter cleaned for 5 min prior to each deposition while the substrate was covered with a protective disc. Single-component nanopillars were grown in a single deposition step while multi-component nanopillars were obtained using alternating Cr and Si deposition. For the latter, a collimating plate covering the substrate was used to prevent any non-directional flux from striking the substrate. Non-directional flux is expected during sputter deposition since the mean-free path of the depositing species in a 1-mTorr Ar atmosphere is  $\sim 5$  cm [32], considerably smaller than the target-substrate distance of 10 cm. The average deposition angle, which is controlled by the substrate position with respect to the targets as well as the height of the collimating plate above the substrate, was chosen to be 84°. However, due to scattering of the deposition flux as well as due to the finite size of the targets, there is a spread in deposition angles of the atoms impinging on the substrate ranging from 83° to 88°, with the majority of the flux being from small angles resulting in the average value for  $\alpha$  of 84°. The deposition angles for single-component nanopillars, grown without the collimating plate, were chosen to be 72° and 86° for Si and Cr, respectively. The substrate holder was rotated about the polar axis at a speed of 60 rpm for the deposition of multi-component nanopillars. Tilted single-component nanopillars were obtained with a fixed substrate. No substrate heating was employed. The temperature, measured by a thermocouple attached to the substrate holder, increases during deposition, due to heating from the plasma discharge, from room temperature to 70 °C. Power-regulated dc power supplies (Advanced Energy-MDX 1.5 K) were used to provide a discharge current of 1.68 A at 597 V for Si and 1.02 A at 494 V for Cr depositions. Cr–Si multi-component nanopillars were deposited at discharge currents of 1.24 A at 411 V and 1.08 A at 455 V for Cr and Si, respectively. The resulting deposition rates, determined using thickness measurements by scanning electron microscopy, ranged from 1.5 to 4 nm/min.

Film microstructures were investigated using a scanning electron microscope (JEOL JSM 6335 Field Emission SEM) operated at 5 kV and an emission current of 12  $\mu$ A. Compositional contrast was achieved using back-scatter electron imaging with a Rutherford Backscattered Electron Imaging (RBEI) detector.

## 3. Results and discussion

Fig. 1 is a plan view SEM micrograph of a Si(001) substrate covered with a monolayer of 500-nm-diameter

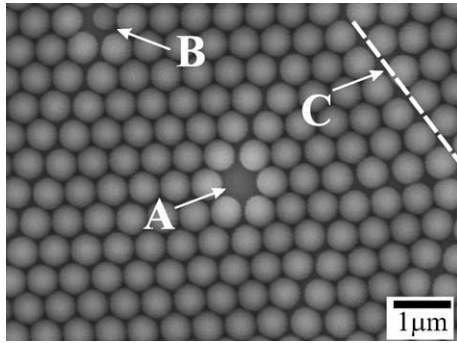


Fig. 1. Scanning electron micrograph from a monolayer of 500-nm-diameter polystyrene microspheres on Si(001), showing a close-packed array including a vacancy (A), a substitutional defect (B), and a grain boundary (C).

polystyrene spheres. The image is obtained with a working distance of 38.9 mm and an electron beam perpendicular to the substrate surface to yield a uniform height-contrast. The micrograph shows a regular, hexagonal close packed array of microspheres with a measured periodicity of 503 nm, close to the nominal sphere diameter of 500 nm. The area of the micrograph was chosen to illustrate crystalline defects in the array of spheres, including a vacancy, a substitutional defect, and a grain boundary labeled with the letters A, B, and C, respectively. Micrograph analyses over large areas (not shown) yield a vacancy concentration of  $4 \times 10^4 \text{ mm}^{-2}$ , corresponding to less than 0.1% of empty lattice sites. The substitutional defect is even less likely, with a density of  $3 \times 10^4 \text{ mm}^{-2}$ . The average grain has a width of 85  $\mu\text{m}$ , corresponding to a grain size of 1800  $\mu\text{m}^2$ , that is, each grain contains an average of  $8 \times 10^4$  microspheres.

The formation of vacancies and grain boundaries is the result of the employed drying process and is affected by the strength of the particle–water–particle interactions [30]. In contrast, the substitutional defects are caused by the size dispersion among the microspheres. The employed dispersion process also yields some large-scale (mm range) defects not shown in Fig. 1. In particular, a fraction of the substrate remains uncovered. In addition, the drying process which starts at the top of the substrate and continues homogeneously towards the bottom causes an accumulation of the colloidal suspension at the bottom of the substrate resulting in the localized deposition of second and third layers as well as microsphere clusters. Accounting for these defects, we obtain on our substrates an overall monolayer coverage of 80%.

Fig. 2 shows SEM micrographs of regular arrays of nanopillar structures grown on substrates patterned using 500-nm-diameter PS microspheres. Fig. 2(a) and (b) are cross-sectional and plan-view micrographs of a silicon nanopillar array grown from a constant angle of  $72^\circ$  with respect to the surface normal without polar substrate rotation. The image in Fig. 2(a) was obtained with the electron beam of the SEM at an angle of  $45^\circ$  to the substrate surface normal to provide a “birds view” of the layer, that

is, this image is rotated with respect to a conventional cross-section. The Si pillars are  $2.14 \pm 0.03 \mu\text{m}$  tall and  $450 \pm 50 \text{ nm}$  wide. The pillars are tilted towards the direction of the incoming deposition flux, which impinges on the substrate from the left back (in Fig. 2(a)). The front of the image shows an area of the substrate with no microspheres, corresponding to an extended patterning defect as described above. This area exhibits no layer growth since the substrate is shadowed during deposition, first by the array of microspheres and then by the growing Si nanopillars.

The Si nanopillars perfectly replicate the close-packed arrangement of the underlying microspheres. Their hexagonal assembly is clearly visible in the plan-view micrograph in Fig. 2(b), showing an average pillar separation of  $520 \pm 20 \text{ nm}$ , in close agreement with 503 nm, the measured distance between microspheres. Fig. 2(c) is a higher magnification micrograph of a Si nanopillar, showing the distinct pillar surface morphology. The surfaces are rough, with protrusions that elongate along the growth direction. We attribute the development of these protrusions to the same shadowing growth instability that causes the formation of the entire nanopillar. That is, small surface irregularities are exacer-

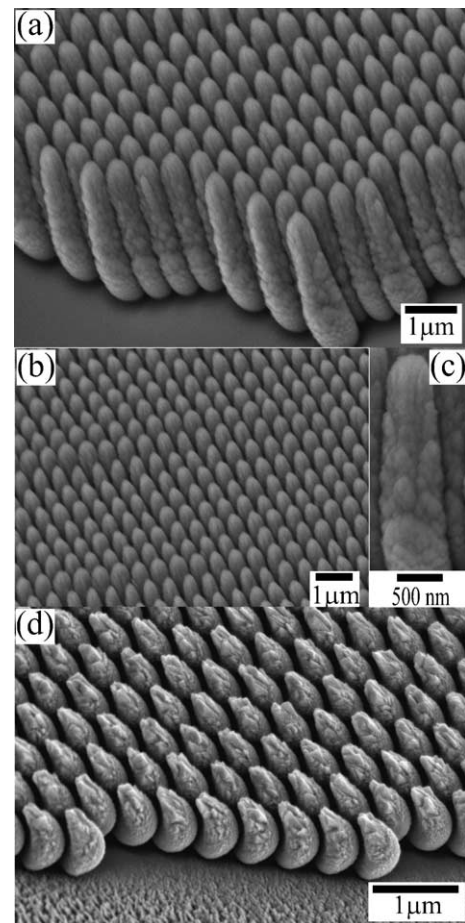


Fig. 2. GLAD nanostructures grown on 500-nm microsphere arrays. (a) side-view, (b) top-view, and (c) high magnification images of Si nanopillars; (d) Cr nano-half-moons.

bated during the growth process since elevations in the surface morphology exhibit an enhanced capturing rate of the deposition flux, yielding locally increased growth rates resulting in surface protrusions. Similar GLAD nanostructure surface morphologies have been reported for cobalt films grown by Dick et al. [33] and silicon films grown by Zhao et al. [34]. Some researchers also found intracolumnar voids and column separations into sub-columns [16,35,36].

The nanopillar shown in Fig. 2(c) was grown on a microsphere at the edge of a pattern, that is, adjacent to an area with a blank substrate, as observed at the front in Fig. 2(a). Consequently, this pillar captures additional deposition flux when compared to nanopillars within a continuous array, since the latter experience atomic shadowing from all their nanopillar-neighbors while the former has fewer neighbors and is less subjected to shadowing. The additional flux to this pillar increases its width which is  $628 \pm 5$  nm near the PS-seed and  $473 \pm 30$  nm near the column top, this is in contrast to nanopillars within the array with constant widths of  $450 \pm 50$  nm.

Fig. 2(d) shows an array of Cr nano-half-moons on 500 nm PS microspheres grown from an angle of  $86^\circ$  with respect to the surface normal. The half-moons are 300 nm wide,  $1.12 \pm 0.05$   $\mu\text{m}$  tall and are well-separated nanostructures. Their unique curved shape is due to the combination of deposition and imaging angles. For this micrograph, the deposition is from the left, slightly from the back. The microsphere-free surface in the front of the image shows some layer growth with a thickness that increases with distance from the sphere pattern. Such growth into the unpatterned defect is expected since, in contrast to the case shown in Fig. 2(a), the deposition flux is primarily from the left so that shadowing of the blank Si substrate by the microsphere array is limited. The micrograph indicates that the nano-half-moons exhibit faceted rough surfaces, suggesting that each nanostructure consists of multiple Cr grains. This is in contrast to the Si nanopillar shown in Fig. 2(c), which exhibits no faceting since room-temperature-grown Si is amorphous.

The micrographs presented in Fig. 2 clearly illustrate that substrate patterning is effective in positioning GLAD nanostructures into ordered arrays, as has been shown previously by several researchers using colloid patterning [34], nanopatterns generated on substrates using TEM [37], and e-beam lithography [16,17]. Each microsphere is the nucleation site for one column. The columns are relatively uniform in height and width, and exhibit rough surfaces. This is typical for GLAD layers with a relatively large spacing between seeds, leading to a suppression of intercolumnar competition, a constant number density of pillars, and rough pillar surfaces due to additional nucleation, as discussed in more detail below.

Fig. 3 shows SEM micrographs of Cr–Si multi-stack nanopillars on 160-nm-diameter  $\text{SiO}_2$  nanospheres. The pillars were grown with continuous rotation of the substrate about the polar axis and using two alternating sequences of

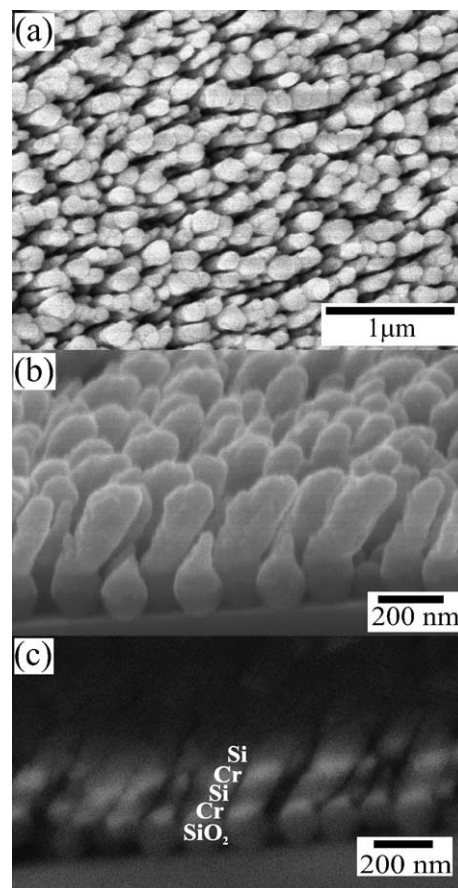


Fig. 3. (a) Plan-view, (b) cross-section, and (c) back-scatter SEM images of Cr–Si multi-component nanopillars grown on 160-nm-diameter silica nanospheres.

Cr and Si deposition steps. The plan-view micrograph in Fig. 3(a) shows that the top-portions of the pillars do exhibit a wide range of width, ranging from 110 to 250 nm, with an average of 150 nm. In addition, their lateral arrangement indicates a relatively random positioning which is in clear contrast to the regular arrays observed for the Si-pillars in Fig. 2. The number density of the nanopillars, as determined from the plan-view micrograph, is  $29 \mu\text{m}^{-2}$ . This is only 64% of  $45 \mu\text{m}^{-2}$ , the calculated nanosphere density of a hexagonal close-packed array with 160 nm spheres. Both the randomness of the nanopillar width and arrangement as well as the reduced nanopillar density with respect to the sphere density can be attributed to a competitive growth mode which leads to the extinction of some pillars, as discussed below.

The cross-sectional micrograph in Fig. 3(b) shows a row of Cr–Si nanopillars with a height of 300 nm. The  $\text{SiO}_2$  nanosphere templates are clearly observable between the Si substrate and the nanopillars. The spheres have a measured diameter of  $155 \pm 6$  nm, in good agreement with the nominal 160 nm. The width of the pillars has a relatively large distribution, from 120 nm to 170 nm. In addition, the average column width also increases as a function of pillar-height, from  $122 \pm 27$  nm near the  $\text{SiO}_2$  spheres to  $150 \pm 17$

nm at the pillar top. The latter value is in good agreement with the average width, 150 nm, obtained from the plan-view micrograph in Fig. 3(a). Two nanostructures shown in the front left of Fig. 3(b) exhibit the opposite trend. Their width decreases as a function of height and their growth terminates early. This observation is in agreement with the finding that the number density of pillars in the plan-view is smaller than that of the microsphere seeds. It also illustrates that these layers are grown in a competitive growth mode, as discussed below. The columns in Fig. 3(b) are tilted towards the right by an angle of  $27^\circ$ . This tilt indicates that a larger fraction of the deposition flux impinges the substrate from the right than from the left. This anisotropy in deposition flux during continuous substrate rotation is related to unintentional off-centering of the substrate with respect to the collimating plate.

Fig. 3(c) is a back-scatter electron image of the same Cr–Si multi-stack nanopillar layer shown in Fig. 3(b). The compositional contrast between  $\text{SiO}_2$ , Si, and Cr is clear from the micrograph. Cr ( $Z=24$ ) has a considerably higher electron back-scattering yield than Si ( $Z=14$ ) and O ( $Z=8$ ). Consequently, the regions of the nanopillars consisting of Cr appear bright while the Si and  $\text{SiO}_2$  are darker, as labeled in the image. This micrograph visualizes that multi-material nanopillar growth by GLAD is feasible.

The nanopillar array morphologies observed in Figs. 2 and 3 are strikingly different: The arrays in Fig. 2 are very regular, with all nanostructures exhibiting comparable height and width, replicating the underlying hexagonal close-packed pattern. In contrast, the array in Fig. 3 shows considerable randomness in pillar width and height, and the pillar arrangement observed in the plan-view micrograph (Fig. 3(a)) does not suggest any hexagonal ordering. We attribute this dramatic change to inter-columnar competition that becomes dramatically exacerbated as the column diameter decreases from 500 to 160 nm. Column competition during GLAD has been investigated by several researchers. Karabacak et al. [28] found, for GLAD on flat substrates, that the column width  $w$  increases with layer thickness  $d$  according to the power law  $w \propto d^p$  with an exponent  $0.28 \leq p \leq 0.34$ . The film density remains constant during any stage of the deposition and hence this increase in the pillar diameter is compensated by a reduction in the number density of the pillars. That is, according to Dick et al. [33], the ratio between pillar diameter and mean pillar separation (this ratio corresponds to the film density) remains constant for a given deposition condition. Kennedy and Brett [38] have shown that the use of complex substrate rotation algorithms allows the suppression of pillar broadening and the reduction of competition effects.

The diameter and separation for GLAD pillars on flat substrates is determined, during the nucleation stage, by the length scales of surface diffusion and self-shadowing. During deposition, competition between neighboring pillars favors the larger ones which grow at the expense of the smaller ones that die out, leading to an increase in width and

decrease in number density of pillars. However, for the case of growth on surface patterns, as in the present investigation, the initial column separations are determined by the pattern dimensions and the competitive growth mode is delayed. In order for the competition to be suppressed, the nanopillar separation needs to be sufficiently large so that the pillar width, determined by surface-diffusion and self-shadowing, can be sustained without disturbing the growth of the neighboring pillar by shadowing. For the deposition conditions of the present investigation, a pillar separation of 500 nm is sufficient to render columnar competition negligible (Fig. 2), while 160 nm separation yields considerable competition resulting in a pillar arrangement (Fig. 3) that resembles those for growth on flat substrates.

#### 4. Conclusions

We have extended the technique of GLAD to create multi-component, multi-stack nanopillars. Cr, Si single component nanopillars, and Cr–Si multi-component nanopillars were grown on Si(001) substrates patterned with 500-nm PS and 160-nm silica microspheres by ultrahigh vacuum DC magnetron sputtering in pure Ar discharges at room temperature. The Si nanopillars grown on 500-nm PS are  $2.13 \pm 0.03 \mu\text{m}$  tall and  $450 \pm 50$  nm wide. The Cr nano-half-moon structures, also grown on 500 nm PS are 300 nm wide, and  $1.12 \pm 0.05 \mu\text{m}$  tall. Cr–Si multi-component nanopillars grown on 160 nm diameter silica nanospheres are 300 nm tall and have their width ranging from 122 nm to 167 nm. Both Si and Cr single-component nanostructures perfectly replicate the hexagonal close-packed arrangement of the underlying 500-nm-diameter microspheres. In contrast, multi-component nanopillar arrays grown on 160-nm spheres exhibit a strikingly different morphology with considerable randomness in pillar width, height and arrangement. We attribute this randomness to a competitive growth mode occurring in 160-nm-spaced patterns yielding a pillar arrangement that resembles those for growth on flat substrates. This competitive growth mode depends on the size and periodicity of the surface pattern and is negligible in the case of 500 nm patterns, which result in highly periodic GLAD nanostructures.

#### Acknowledgements

This research was supported by the National Science Foundation, Division of Manufacturing and Industrial Innovation, under grant No. DMII-0423358 and DMII-0304028.

#### References

- [1] N.O. Young, J. Kowal, Nature 183 (1959) 104.
- [2] K. Robbie, M.J. Brett, A. Lakhtakia, Nature 384 (1996) 616.

- [3] K. Robbie, D.J. Broer, M.J. Brett, *Nature* 399 (1999) 764.
- [4] R. Messier, V.C. Venugopal, P.D. Sunal, *J. Vac. Sci. Technol.*, A 18 (2000) 1528.
- [5] K. Robbie, M.J. Brett, *J. Vac. Sci. Technol.*, A 15 (1997) 1460.
- [6] K. Robbie, J.C. Sit, M.J. Brett, *J. Vac. Sci. Technol.*, B 16 (1998) 1115.
- [7] A. Lakhtakia, *Mater. Sci. Eng.*, C 19 (2002) 427.
- [8] M. Suzuki, Y. Taga, *J. Appl. Phys.* 71 (1992) 2848.
- [9] I.J. Hodgkinson, Q.H. Wu, *Appl. Opt.* 38 (1999) 3621.
- [10] I.J. Hodgkinson, Q.H. Wu, *Opt. Eng.* 37 (1998) 2630.
- [11] K. Robbie, M.J. Brett, A. Lakhtakia, *J. Vac. Sci. Technol.*, A 13 (1995) 2991.
- [12] R.M.A. Azzam, *Appl. Phys. Lett.* 61 (1992) 3118.
- [13] A. Lakhtakia, R. Messier, *Optics Photonics News* (2001 (Sept. 01)) 27.
- [14] I.J. Hodgkinson, Q.H. Wu, K.E. Thorn, A. Lakhtakia, M.W. McCall, *Opt. Commun.* 184 (2000) 57.
- [15] M. Malac, R.F. Egerton, *J. Vac. Sci. Technol.*, A 19 (2001) 158.
- [16] M. Malac, R.F. Egerton, M.J. Brett, B. Dick, *J. Vac. Sci. Technol.*, B 17 (1999) 2671.
- [17] M. Malac, R.F. Egerton, *Nanotechnology* 12 (2001) 11.
- [18] A. Lisfi, J.C. Lodder, *Phys. Rev.*, B 63 (2001) 174441.
- [19] R.D. McMichael, C.G. Lee, J.E. Bonevich, P.J. Chen, W. Miller, W.F. Egelhoff Jr., *J. Appl. Phys.* 88 (2000) 3561.
- [20] B. Dick, M.J. Brett, T.J. Smy, M.R. Freeman, M. Malac, R.F. Egerton, *J. Vac. Sci. Technol.*, A 18 (2000) 1838.
- [21] A. Hagemeyer, H.J. Richter, H. Hibst, V. Maier, L. Marosi, *Thin Solid Films* 230 (1993) 199.
- [22] K. Starbova, J. Dikova, N. Starbov, *J. Non-Cryst. Solids* 210 (1997) 261.
- [23] A. Sugawara, T. Coyle, G.G. Hembree, M.R. Scheinfein, *Appl. Phys. Lett.* 70 (1997) 1043.
- [24] Y.-P. Zhao, D.-X. Ye, P.-I. Wang, G.-C. Wang, T.-M. Lu, *Int. J. Nanosci.* 1 (2002) 87.
- [25] Y.-P. Zhao, D.-X. Ye, G.-C. Wang, T.-M. Lu, *Nano Lett.* 2 (2002) 351.
- [26] J.P. Singh, F. Tang, T. Karabacak, T.-M. Lu, G.-C. Wang, *J. Vac. Sci. Technol.*, B 22 (3) (2004) 1048.
- [27] B. Dick, M.J. Brett, T. Smy, M. Belov, M.R. Freeman, *J. Vac. Sci. Technol.*, B 19 (5) (2001) 1813.
- [28] T. Karabacak, J.P. Singh, Y.-P. Zhao, G.-C. Wang, T.-M. Lu, *Phys. Rev.*, B 68 (2003) 125408.
- [29] J. Lintymer, J. Gavaille, N. Martin, J. Takadoum, *Surf. Coat. Technol.* 174–175 (2003) 316.
- [30] R. Micheletto, H. Fukuda, M. Ohtsu, *Langmuir* 11 (1995) 3333.
- [31] W. Kern, D.A. Puotinent, *RCA Rev.* 31 (1970) 187.
- [32] M. Ohring, *Materials Science of Thin Films*, 2nd ed., Academic Press, London, 2002.
- [33] B. Dick, M.J. Brett, T. Smy, *J. Vac. Sci. Technol.*, B 21 (1) (2003) 23.
- [34] Y.-P. Zhao, D.-X. Ye, P.-I. Wang, G.-C. Wang, T.-M. Lu, *Int. J. Nanosci.* 1 (2002) 87.
- [35] C. Rol, H. Guo, *Phys. Rev. Lett.* 66 (1991) 2104.
- [36] J.H. Yao, C. Roland, H. Guo, *Phys. Rev. Lett.* A 45 (1992) 3903.
- [37] M. Malac, R.F. Egerton, *Nanotechnology* 12 (2001) 11.
- [38] S.R. Kennedy, M.J. Brett, *J. Vac. Sci. Technol.*, B 22 (3) (2004) 1184.